Published in final edited form as:
Sci Signal. ; 2(101): ra82. doi:10.1126/scisignal.2000446.

EGFR Signaling Through an Akt-SREBP-1-Dependent, Rapamycin-Resistant Pathway Sensitizes Glioblastomas to Anti-Lipogenic Therapy

Deliang Guo[1], **Robert M. Prins**[2], **Julie Dang**[1], **Daisuke Kuga**[1], **Akio Iwanami**[1], **Horacio Soto**[2], **Kelly Y. Lin**[1], **Tiffany T. Huang**[1], **David Akhavan**[1], **M. Benjamin Hock**[1], **Ava A. Kofman**[1], **Steve J. Bensinger**[1], **William H. Yong**[1,3], **Harry V. Vinters**[1,4], **Steve Horvath**[5], **Andrew D. Watson**[6], **John G. Kuhn**[7], **H. Ian Robins**[8], **Minesh P. Mehta**[8], **Patrick Y. Wen**[9], **Lisa M. DeAngelis**[10], **Michael D. Prados**[11], **Ingo K. Mellinghoff**[10], **Timothy F. Cloughesy**[3,4], and **Paul S. Mischel**[1,3,12,†]

[1]Departments of Pathology & Laboratory Medicine, The David Geffen UCLA School of Medicine, Los Angeles

[2]Department of Surgery, Division of Neurosurgery, The David Geffen UCLA School of Medicine, Los Angeles

[3]The Henry Singleton Brain Tumor Program and The Jonsson Comprehensive Cancer Center, The David Geffen UCLA School of Medicine, Los Angeles

[4]Department of Neurology, The David Geffen UCLA School of Medicine, Los Angeles

[5]Departments of Human Genetics and Biostatistics, The David Geffen UCLA School of Medicine, Los Angeles

[6]Department of Medicine, Division of Cardiology, The David Geffen UCLA School of Medicine, Los Angeles

[7]University of Texas Health Science Center at San Antonio, San Antonio, TX

[8]University of Wisconsin-Madison, Madison, WI

[9]Dana Farber Cancer Institute, Boston, MA

[10]Memorial Sloan-Kettering Cancer Center, New York, NY

[11]University of California, San Francisco, San Francisco, CA

[12]Molecular & Medical Pharmacology, The David Geffen UCLA School of Medicine, Los Angeles

Abstract

Glioblastoma, the most common malignant brain tumor, is among the most lethal and difficult cancers to treat. Although epidermal growth factor receptor (EGFR) mutations are frequent in glioblastoma, their clinical relevance is poorly understood. Studies of tumors from patients treated with the EGFR-inhibitor lapatinib revealed that EGFR induces the cleavage and nuclear translocation of the master transcriptional regulator of fatty acid synthesis, sterol regulatory element-binding protein 1 (SREBP-1). This response was mediated by Akt; however, clinical data from rapamycin-treated patients showed that SREBP-1 activation was independent of the mammalian target of rapamycin complex 1 (mTORC1), possibly explaining rapamycin's poor efficacy in the treatment of such tumors. Glioblastomas without constitutively active EGFR signaling were resistant to inhibition of

[†]To whom correspondence should be addressed. pmischel@mednet.ucla.edu.

fatty acid synthesis, whereas introduction of a constitutively active mutant form of EGFR, EGFRvIII, sensitized tumor xenografts in mice to cell death, which was augmented by the hydroxymethylglutaryl-CoA (HMG-CoA) reductase inhibitor atorvastatin. These results identify a previously undescribed EGFR-mediated pro-survival metabolic pathway, and suggest new therapeutic approaches to treating EGFR-activated glioblastomas.

INTRODUCTION

Glioblastomas (GBMs) aggressively invade the surrounding brain, making complete surgical excision impossible. Unfortunately, GBMs are also among the most radiation- and chemotherapy-resistant of all cancers. On average, GBM patients survive 12 to 15 months from the time of initial diagnosis (1,2). The epidermal growth factor receptor (EGFR), which is amplified in up to 45% of GBM patients (3), has oncogenic activity (4,5). However, EGFR inhibitors have been ineffective in the clinic (6). Maintenance of signal flux through the phosphatidylinositol-3-kinase (PI3K)-Akt-mammalian target of rapamycin complex 1 (mTORC1) pathway, either as a consequence of PTEN (phosphatase and tension homolog deleted from chromosome 10) loss (7,8), a key negative regulator of PI3K signaling, or through co-activation of other receptor tyrosine kinases (RTKs) (9), together with failure to block EGFR-mediated changes in cellular metabolism, have been suggested as possible explanations for the resistance of multiple cancers, including GBMs, to inhibitors of EGFR tyrosine kinase activity (10–13). However, attempts to determine the clinical importance of EGFR signaling in GBM have been hampered by a lack of studies designed to assess the acute effects of EGFR inhibitors on signal transduction and tumor metabolism in patients. Here we analyzed GBM clinical samples, cell lines and a mouse model to identify an EGFR- and Akt-dependent, rapamycin-insensitive signaling pathway that promotes GBM cell survival through sterol regulatory element-binding protein 1 (SREBP-1) -dependent fatty acid synthesis.

RESULTS

Inhibition of EGFR-PI3K-Akt signaling suppresses SREBP-1 nuclear translocation in GBM patients treated with lapatinib

As part of a Phase II clinical trial for the EGFR inhibitor lapatinib, we performed quantitative immunohistochemical analysis of tumor tissue from the first nine GBM patients for whom tissue was available both at initial diagnosis (surgery 1) and after a 7 to 10 day course of treatment (surgery 2) (Fig. 1A). We have previously demonstrated the effectiveness of this assay in measuring drug-specific effects in GBM patients (14). Access to pre- and post-treatment samples for each patient facilitated intra-patient comparison of molecular endpoints, enhancing the statistical power to detect changes in this small sample size. Immunohistochemical staining for EGFR phosphorylated on Tyr^{1086} (p-EGFR), a measure of EGFR activation (Fig. 1, B and C), was significantly decreased in tumors from lapatinib-treated patients ($p<0.05$). Decreased p-EGFR was detected in tumors from 6 of 9 patients (Fig. 1D), with increased intra-tumor lapatinib concentration in tumors that demonstrated decreased EGFR phosphorylation (table S1). Staining for Akt phosphorylated on Ser^{473} (p-Akt), a measure of PI3K pathway activity (15), was also significantly decreased after lapatinib treatment ($p<0.01$) (Fig. 1, B and C), consistent with the decrease in p-EGFR ($p<0.01$) (Fig. 1D). Thus, lapatinib inhibited EGFR signaling through Akt in glioblastomas from the majority of patients examined.

PI3K signaling is associated with increased fatty acid synthesis (16), therefore we examined the effect of lapatinib on SREBP-1, the master transcriptional regulator of fatty acid synthesis. SREBP-1 undergoes N-terminal cleavage and nuclear translocation in response to cholesterol and fatty acid deprivation to initiate transcription of fatty acid-synthetic genes (17,18).

Quantitative image analysis demonstrated a significant reduction in the percentage of nuclei staining positively for SREBP-1 between surgery 1 (before) and surgery 2 (after) in tumor specimens from lapatinib-treated patients (Fig. 1, B–D). This reduction in SREBP-1 nuclear staining was highly correlated with decreased p-EGFR immunostaining (R^2=0.73, p< 0.00001) (Fig. 1E). To provide confidence that the reduction in immunohistochemical nuclear staining for SREBP-1 was attributable to lapatinib, we made an identical set of measurements on tissue from 12 GBM patients from whom tumor tissue was available at baseline and at recurrence, but who did not receive lapatinib (controls). No reduction in the percent of nuclei staining positively for SREBP-1 between surgery 1 and 2 was detected in these control GBM patients (fig. S1). Thus, inhibition of EGFR signaling resulted in significantly reduced nuclear SREBP-1 staining of tumor tissue from lapatinib-treated GBM patients. Consistent with a role for Akt in mediating EGFR-dependent nuclear translocation of SREBP-1, nuclear SREBP-1 staining was diminished when PTEN staining was apparent in p-EGFR-expressing tumors (fig. S2).

Rapamycin does not suppress SREBP-1 nuclear translocation in GBM patients

mTORC1 has been shown to mediate PI3K-Akt-dependent SREBP-1 cleavage to promote cell growth in vitro and in a *Drosophila* model (19). Therefore, we examined tumor tissue from a cohort of 9 recurrent GBM patients treated with rapamycin in a Phase I/II clinical trial (14) (Fig. 1F). We previously demonstrated significant inhibition of phosphorylation of the mTORC1 target S6 in these patients ($P < 0.05$) (Fig. 1, G and H) (14). However, mTORC1 inhibition did not correlate with reduced SREBP-1 nuclear staining (Fig. 1, G and H). Thus, in GBM patients, the amount of nuclear SREBP-1 staining was unaffected by rapamycin treatment at doses that inhibited mTORC1 signaling through S6.

EGFR-PI3K-Akt signaling promotes SREBP-1 cleavage and increases fatty acid concentration in GBM cells

To assess the effect of EGFR signaling on SREBP-1 cleavage, we pharmacologically and genetically manipulated GBM cell lines at multiple nodes in the EGFR-PI3K-Akt signaling pathway. Substantially more cleaved SREBP-1 was detected in two of two cell lines with large amounts of p-EGFR (Fig. 2A, lanes 1, 6) than in four of four cell lines with little p-EGFR (Fig. 2A, lanes 2–5); this did not appear to directly correlate with proliferation rate (fig. S3). The presence in U87 cells of a constitutively active EGFR allele, the EGFRvIII mutant, potently increased Akt phosphorylation and was sufficient to promote SREBP-1 cleavage as well as increased concentrations of fatty acid (Fig. 2, B and C). EGF stimulation of glioblastoma cells expressing wild-type EGFR elicited a dose- and time-dependent increase in SREBP-1 cleavage (Fig. 3, A and B), which was detectable 4 hours after EGF stimulation and was preceded by increased Akt Ser^{473} and Thr^{308} site phosphorylation (Fig. 3B). 25-hydroxycholesterol (25-HC) (1 μg/ml), an inhibitor of SREBPs processing (18,20–23) abrogated EGF-induced SREBP-1 cleavage (fig. S4). To determine whether increased SREBP-1 cleavage in response to EGF stimulation resulted in increased transcriptional regulation of the SREBP-1 transcriptional target fatty acid synthase (FAS), we performed chromatin immunoprecipitation (ChIP) analysis. SREBP-1 binding to the FAS promoter at the TSS was increased 6.7 times (p<0.02) 4 hours after addition of EGF, whereas no increase in SREBP-1 binding to the FAS TSS was detected in vehicle-treated cells (Fig. 3, C and D). Furthermore, no SREBP-1 binding was detected to a site 200 base pairs (bp) upstream of the FAS TSS (Fig. 3, C and D). The EGFR inhibitor erlotinib, the PI3K inhibitor LY294002, and the Akt inhibitor Akti-1/2, all blocked EGF-stimulated SREBP-1 cleavage (Fig. 3E). U87-EGFRvIII cells lack PTEN; its introduction into cell line through retrovirus infection also abolished SREBP-1 cleavage (Fig. 3F). Rapamycin did not prevent EGFR-mediated SREBP-1 cleavage despite its inhibition of mTORC1 as assessed by the decrease in S6 phosphorylation (Fig. 3E, fig. S5), consistent with our findings in rapamycin-treated patients (Fig. 1, G and H). Thus, in GBM cells, EGFR

signaling through PI3K-Akt promotes SREBP-1 cleavage, initiates binding of cleaved SREBP-1 to the FAS promoter, and increase intracellular fatty acid concentration in a process that does not depend on mTORC1 activity.

Identification of molecular circuitry linking EGFR-Akt signaling with SREBP-1 in a large cohort of GBM patients

We examined the frequency with which we could detect p-EGFR, p-Akt, and nuclear SREBP-1, as well as acetyl coenzyme A (CoA) carboxylase (ACC) and FAS, two pivotal enzymes of the fatty acid synthetic pathway that are regulated by SREBP-1, in multiple representative regions of tumor and adjacent normal tissue from 140 patients with primary GBMs, that is, GBMs that had not transformed from lower grade gliomas (Fig. 4A). P-EGFR and p-Akt were detected in 44% and 77% of the tumor samples, respectively (table S2). This is consistent with the finding of EGFR mutation and/or amplification in 45% and PI3K-pathway activating mutations in 87% of primary GBMs respectively (3), suggesting that we had analyzed a representative patient population. Nuclear SREBP-1 and ACC and FAS staining were also significantly increased in tumor tissue relative to normal brain ($p<0.0001$ for each) (table S2) and were highly correlated with each other ($p<0.0001$ for each comparison); with p-Akt ($p<0.0001$ for each), and with p-EGFR ($p<0.0001$ for each) (tables S3 and S4).

To determinate if this dataset might be used to uncover a signaling pathway linking EGFR signaling through PI3K-Akt to activation of SREBP-1 in patients, we used a classical multidimensional scaling (MDS) plot to visualize the pair-wise correlations between p-EGFR, p-Akt, SREBP-1, ACC and FAS (15,24). MDS is an unsupervised data analysis method that does not assume previous knowledge about the interaction patterns between the proteins analyzed. The closer the distance between proteins in the MDS plot, the more correlated their expression in the 140 tumor samples. The MDS plot suggests a pattern of correlation between EGFR-Akt signaling and the SREBP-1-ACC-FAS fatty synthesis pathway (Fig. 4B) that is consistent with the pre-clinical observations (Fig. 3) and with the observations in the lapatinib treated patients (Fig. 1). These results indicate that EGFR-Akt signaling is tightly correlated with SREBP-1, ACC and FAS in clinical GBM samples.

Immunoblot analysis from autopsies of three GBM patients for whom tumor tissue and contralateral normal brain tissue were available demonstrated increased SREBP-1 cleavage and ACC and FAS abundance in tumor tissue relative to normal brain, as well as increased EGFR and Akt phosphorylation (Fig. 4, C and D). Thus, in a representative cohort of GBM patients, p-EGFR was associated with increased p-Akt, nuclear SREBP-1 staining, and increased abundance of enzymes of the fatty acid biosynthetic pathway. Other RTKs that can activate Akt signaling, such as platelet-derived growth factor receptor (PDGFR) and mesenchymal-epithelial transition factor (MET), can also be found in GBM (9). Both p-PDGFR and p-MET correlated with SREBP-1 in glioblastoma (fig. S6, table S4). Addition of hepatocyte growth factor (HGF) to glioblastoma cells carrying MET promoted SREBP-1 cleavage (fig. S6C), suggesting that other RTKs besides EGFR can also activate this pathway.

Short hairpin RNA–mediated knockdown of SREBP-1 promotes cell death of EGFRvIII-bearing GBM cells

Having demonstrated that EGFR signaling through Akt can promote SREBP-1 cleavage and that EGFR and Akt phosphorylation correlates with SREBP-1 nuclear localization in tumors from GBM patients, we assessed the requirement for SREBP-1 in EGFR-activated cultured GBM cell line using a genetic approach. U87 and U87-EGFRvIII cells were infected with an SREBP-1 Short hair-carrying lentivirus, or with a lentivirus carrying scrambled control Short hair, and the effect on downstream SREBP-1 targets, and on cell proliferation and viability was measured (Fig. 5, A and B). SREBP-1 knockdown resulted in decreased abundance of

ACC and FAS (Fig. 5A) and inhibition of cell proliferation (Fig. 5B), with slightly more inhibition of proliferation in U87-EGFRvIII cells than in U87 cells. However, genetic inhibition of SREBP-1 resulted in massive cell death in U87-EGFRvIII cells maintained in medium containing 1% Fetal bovine Serum (FBS) for 4 days, an effect that was not observed with parental U87 GBM cells (Fig. 5, C and D). Thus, EGFRvIII-bearing GBM cells demonstrated enhanced dependence on SREBP-1 for survival in low concentration of Fetal bovine Serum (FBS).

Inhibition of lipogenesis promotes EGFR-activated tumor cell death in vitro and in vivo

To assess the possible therapeutic consequences of pharmaceutical inhibition of the Akt-SREBP-1 pathway, and to determine whether its inhibition can promote the death of tumor cells with high degrees of EGFR signaling, we treated a panel of GBM cell lines with 25-HC (1 μg/ml for 3 days) (Fig. 6, A–C, figs. S7–9). 25-HC caused massive cell death in tumors with large amounts of p-EGFR (Fig. 6B, figs. S7–9); minimal cell death was detected in GBM cell lines with little of p-EGFR (Fig. 6C, fig. S7A). Cell death in response to 25-HC (1 μg/ml for 3 days in 1% FBS) was enhanced in U87-EGFRvIII cells relative to that in U87 cells (fig. S7C), an effect that was abrogated by PTEN (fig. S10). Thus, EGFR signaling through the PI3K pathway can sensitize GBM cells to the effects of 25-HC. To determine whether sensitivity to 25-HC depended on inhibition of cholesterol synthesis or of fatty acid synthesis, we treated GBM cells containing varying amounts of p-EGFR with the HMG-CoA reductase inhibitor atorvastatin (1 μM), to inhibit cholesterol synthesis and the FAS inhibitor C75 (10 μg/ml), to inhibit fatty acid production. Atorvastatin did not promote cell death, regardless of EGFR status (Fig. 6, B and C). In contrast, C75 caused cell death in cell lines with abundant p-EGFR but had significantly less effect on the cells with little p-EGFR (Fig. 6, B and C, figs. S8 and S9). The apoptotic effect of C75 on cell lines with abundant p-EGFR was significantly rescued by addition of palmitate, an end product of FAS enzymatic activity (fig. S11). Thus, EGFR signaling markedly enhances demand for fatty acid synthesis necessary for the survival of GBM cells.

To determine whether constitutively active EGFR signaling was sufficient to impose enhanced dependence of GBM on lipogenesis in vivo, we implanted U87 and U87-EGFRvIII cells into opposite flanks of immunodeficient SCID/Beige mice (Fig. 6D). EGFRvIII-containing tumors grew significantly larger compared to tumors without EGFRvIII (Fig. 6, E and F), with increased Ki67 proliferation indices (fig. S12), and lower apoptotic indices (Fig. 6, G and H) (25). Atorvastatin did not inhibit tumor growth in either U87 or U87-EGFRvIII tumors (Fig. 6, E and F, fig. S12). In contrast, C75 significantly inhibited tumor growth and promoted apoptosis, showing greatly enhanced efficacy in EGFRvIII-bearing tumors compared to those without EGFRvIII (Fig. 6, E–H, fig. S13). The effects of atorvastatin and C75 on tumor cell proliferation were modest (fig. S12). Atorvastatin augmented the apoptotic effect of C75 (Fig. 6, G and H). Therefore, a persistently active EGFR allele sensitized GBMs to apoptotic cell death in response to lipogenic inhibitors in vitro and in vivo (Fig. 7).

DISCUSSION

Our analysis of clinical samples from patients before and after treatment with lapatinib combined with our studies in cell lines and a mouse model, has enabled us to identify an EGFR- and Akt-dependent, rapamycin-insensitive signaling pathway that promotes GBM cell survival by bridging oncogenic growth factor receptor signaling with altered cellular metabolism (Fig. 7) (16,26–29). Our data also support the recent demonstration that FAS suppresses tumor cell apoptosis in prostate cancer (30) and suggest a strategy for treating GBMs carrying constitutively activated, and possibly other cancers carrying activated EGFR, by targeting lipogenesis (31). Attempts to treat GBMs with constitutively active EGFR signaling by

inhibiting EGFR itself have been limited because of resistance mediated by maintained signaling through the PI3K-Akt pathway (9,14). It is not yet clear whether lapatinib will be subject to the same pitfalls; the first phase analysis of the lapatinib clinical trial cannot answer that question. However, because fatty acid synthesis is downstream of EGFR-PI3K signaling, it is unlikely that rewiring of the pathway upstream, either through co-activation of other RTKs, or by selection for loss of the tumor suppressor PTEN will promote resistance to anti-lipogenic therapy. Increased EGFR signaling through PI3K-Akt enhances the requirement of GBM cells for fatty acid synthesis, possibly to provide sufficient lipids for membrane biogenesis in rapidly dividing tumor cells. This demand for increased fatty acids is met by EGFR-PI3K-Akt-mediated activation of SREBP-1 cleavage and upregulation of ACC and FAS. Therefore, targeting SREBP-1, ACC and FAS is lethal to GBM cells with abundant EGFR signaling, but spares cells with little EGFR signaling, including normal cells (Fig. 7). These results define a therapeutically exploitable synthetic lethal interaction (32), i.e. SREBP-1-ACC-FAS becomes essential for survival when EGFR is constitutively activated, explaining the specificity of the effect of C75 on EGFRvIII-bearing tumors. It will be important to determine whether targeting fatty acid synthesis results in more effective therapy for GBM patients, and potentially other cancer patients with EGFR-dependent tumors.

MATERIALS AND METHODS

Clinical trial and Patient eligibility

Phase II Lapatinib Clinical Trial—North American Brain Tumor Consortium (NABTC) trial 04-01 titled A Biomarker and Phase II study of GW 572016 (lapatinib) in Recurrent Malignant Glioma enrolled consented patients from University of California at Los Angeles, University of San Francisco, Dana-Farber Cancer Center, Memorial Sloan Kettering Cancer Center, University of Pittsburgh, Neuro-oncology Branch of National Institutes of Health, University of Wisconsin and Duke University. Adult patients who had a Karnofsky performance score (KPS) equal to or greater than 60, who were not on enzyme-inducing anti-epileptic agents, and who had normal hematologic, metabolic, and cardiac function were eligible for this study. In addition, patients must have been candidates for surgical re-resection at the time of enrollment. Patients were administered 750 mg of lapatinib orally twice a day (BID) for 7 to10 days (depending on whether treatment interval fell over a weekend) prior to surgery, the time to steady-state. Blood and tissue samples were obtained at the time of resection. After recovery from surgery, patients resumed lapatinib treatment at the neoadjuvant dose 750 mg BID until clinical or radiographic evidence for tumor progression was found. A complete description of the clinical trial results will be reported separately. The first cohort of patients for whom tissue was available before and after lapatinib (n=9) were included this study.

Lapatinib concentration in peripheral blood and tumor tissue—Blood and tissue samples (minimum 50 mg) were obtained at time of resection. Lapatinib concentrations were determined by liquid chromatography electrospray ionization tandem mass spectrometry (LC/MS/MS) (33), with a lower limit of detection in plasma of 5 ng/mL, and in brain tumor tissue extracts of 0.08 ng/mL.

Phase I/II Rapamycin Clinical Trial—The clinical trial protocol (#02-03-078–11) was approved by the Institutional Review Board of the University of California Los Angeles. Enrollment was restricted to patients with a histological diagnosis of glioblastoma (GBM), radiographic evidence for disease recurrence after standard GBM therapy (surgery, radiation, temozolamide), evidence for PTEN loss in tumor tissue, and no previous mTOR inhibitor therapy. Other enrollment criteria included age > 18 year old, Karnofsky performance score (KPS) ≥ 60, life expectancy ≥ 8 wk, normal hematologic and metabolic function in addition, limitations were placed upon baseline levels of plasma cholesterol and triglycerides. Irradiation

and chemotherapy were discontinued for ≥ 4 wk before trial entry (≥ 6 wk if prior therapy included a nitrosourea compound). All 15 patients enrolled in the clinical trial gave written informed consent to participate in these evaluations.

Fifteen patients with PTEN-deficient tumors, who also met all other eligibility criteria, were enrolled at the time of tumor recurrence and received neoadjuvant oral daily rapamycin (2 mg, 5 mg, or 10 mg/d) for approximately 1 wk (median: 6 d, mean: 7.5 d) prior to salvage surgical resection (S2). After recovery from surgery, patients resumed daily rapamycin treatment at the neoadjuvant dose until clinical or radiographic evidence for tumor progression was found. Details regarding the results from this trial are published in Cloughesy TF, *et al*. (14). Pre- and post-treatment tissue samples were available for analysis in this study from 9 patients.

Cell lines—U87 and U87-EGFRvIII, U87-EGFR, U87-EGFRvIIII-PTEN isogenic glioblastoma cell lines, A431 epidermoid carcinoma cell line, and LN229, T98, U138, U373 glioblastoma cell lines were cultured in DMEM (Cellgro) supplemented with 10% FBS (Omega Scientific) in a humidified atmosphere of 5% CO_2, 95% air at 37°C. U87-EGFRvIII cells were a kind gift of Dr. Webster Cavenee. U87-EGFRvIII-PTEN cells were generated by plasmid-mediated transfection of PTEN into U87-EGFRvIII cells followed by selection for stable clones. U87-EGFR cells were generated by retrovirus-mediated transduction of wild-type EGFR into U87 cells followed by selection of stable clones. These cell lines have previously been reported (7). H1975 Non-small cell lung carcinoma cell line was cultured in RPMI1640 with 10% FBS.

Antibodies and Reagents—We used antibodies directed against the following: ACC, FAS, p-Akt Ser^{473}, p-Akt Thr^{308}, Akt, p-S6 $^{Ser235/236}$, p-Met Tyr^{1234}, p-PDGFR Tyr^{1021}, p-GSK3beta Ser^{9}, PTEN (Cell Signaling); α-actin (Sigma); SREBP-1 (BD Pharmingen); p-Met Tyr^{1349}, p-PDGFR Tyr^{579} (Abgent); EGFR/EGFRvIII cocktail antibody (Upstate); phospho-EGFR Tyr^{1086} (Invitrogen), PTEN (6H2.1, Cascade BioScience, IHC). Reagents used are LY294002 and 25-hydroxycholesterol, C75, Rapamycin, Palmitate, Polybrene (Sigma); Erlotinib (ChemieTex), Akti-1/2 (Calbiochem). Atorvastatin (Toronto Research Chemicals, Canada).

Cell Proliferation and Death Assays—Cells were seeded in 96 wells and were treated after 24 hours with different drugs indicated in each experiment in medium containing 1% FBS. Relative proliferation to control cells with vehicle treatment was checked using Cell Proliferation Assay Kit (Chemicon). Cells were incubated 1.5 hrs after adding tetrazolium salt WST-1 [2-(4-iodophenyl)-3-(4-nitrophenyl)-5-(2, 4-disulfo-phenyl)-2H-tetrazolium, monosodium salt] (Chemicon) at 5% CO^2, 37°C and the absorbance of the treated and untreated cells were measured using a microplate reader (Bio-Rad) at 420 to 480 nm. Cell death was assessed by trypan blue exclusion (Invitrogen).

ShRNA assay—5×10^4 cells were seeded in 12 well plates and maintained for 24 hrs, after which medium was replaced with fresh 5% FBS medium including 5 ug/ml Polybrene (Sigma), and then shRNA lentivirus was added to cells, followed by incubation for 24 hrs. For Western blot analysis, infected cells were incubated in fresh 5% FBS medium for another 24 hrs, then lysed. For cell proliferation or cell death assays, infected cells were subcultured into 96 well plates or 12 well plates, maintained in 5% FBS medium for 24 hrs, then changed to 1% FBS medium and maintained for 4 to 5 days.

Western Blotting—Western blotting was as previously described (34). Cultured cells or snap-frozen tissue samples were lysed and homogenized using buffer containing 10 mmol/L Tris, pH 7.4, 100 mmol/L NaCl, 1 mmol/L EDTA, 1 mmol/L EGTA, 1 mmol/L NaF, 20 mmol/L $Na_4P_2O_7$, 2 mmol/L Na_3VO_4, 0.1% sodium dodecyl sulfate, 0.5% sodium deoxycholate, 1%

Triton X-100, 10% glycerol, 10 μg/mL leupeptin, 60 μg/mL aprotinin, and 1 mmol/L phenylmethanesulfonyl fluoride. Equal amounts of protein extracts were separated by using 8% or 10% SDS-PAGE, and then transferred to a polyvinylidene difluoride membrane (Bio-Rad Laboratories Inc, Hercules, Calif). After blocking for 1 hour in a Tris-buffered saline containing 0.1% Tween 20 and 5% nonfat milk, the membrane was probed with various primary antibodies, followed by secondary antibodies conjugated to horseradish peroxidase. The immunoreactivity was revealed by use of an ECL kit (Amersham Biosciences Co., Piscataway, NJ).

Thin Layer Chromatography for Lipids—Cellular total lipid extract was obtained by scraping cells from the 10 cm culture dish into 2 ml PBS containing protease inhibitor and 1 mM phenylmethylsulphonyl fluoride (PMSF) and adding 4 ml of chloroform/methanol (2:1, v/v) with 0.01% butylated hydroxytoluene (Sigma). The solution was vortexed and centrifuged at 1500 g for 5 min. The organic phase was collected and 2.5 ml of chloroform was added to the residual aqueous phases which was vortexed and centrifuged at 1500 g for 5 min. The organic phase was pooled with the previous extraction. Thin layer chromatography (TLC) was performed by spotting the cellular total lipid extract on a 5 × 10 cm silica gel aluminum sheet (EMD Chemicals) and developed with hexane/diethyl ether/acetic acid (80:20:2, v/v/v). Lipids were visualized with iodine vapor and imaged using a desktop scanner (31,35).

Immunohistochemical and Immunofluorescent Staining—Paraffin-embedded tissue blocks were sectioned using the UCLA Pathology Histology and Tissue Core Facility. Immunohistochemical staining (IHC) was performed as previously described (7). Slides were counterstained with hematoxylin to visualize nuclei. Paraffin-embedded tissue sections underwent immunohistochemical analysis in which the results were scored independently by two pathologists who were unaware of the findings of the molecular analyses. Quantitative image analysis to confirm the pathologists' scoring was also performed with Soft Imaging System software (15). We have previously demonstrated the utility of this quantitative method for measuring drug-specific effects in paraffin-embedded tissue samples from GBM patients enrolled in clinical trials with targeted agents (7,14).

Tissue Microarrays—Tissue microarrays (TMAs) were used to analyze p-EGFR Tyr^{1086}, p-Akt Ser^{473}, nuclear SREBP-1, ACC and FAS immunohistochemical staining in 140 GBM patient samples. Tissue microarrays (TMAs) enable tumor tissue samples from hundreds of patients to be analyzed on the same histologic slide. We constructed two GBM TMAs by using a 0.6 mm needle to extract 252 representative tumor tissue cores and 91 adjacent normal brain tissue cores from the paraffin-embedded tissue blocks of 140 primary GBM patients. These cores were placed in a grid pattern into two recipient paraffin blocks, from which tissue sections were cut for immunohistochemical analysis of p-EGFR, p-Akt, nuclear SREBP-1, ACC and FAS. These TMAs have been used for other studies (15,36).

TUNEL Staining—Paraffin sections were deparaffinized and subjected to graded rehydration as with the immunohistochemical method. Peroxidase activity was quenched with 3% hydrogen peroxide in water. TUNEL staining was performed using digoxigenin-conjugated dUTP and HRP-conjugated anti-digoxigenin antibodies following its protocol (Roche). Visualization for staining was performed with NovaRed substrate (Vector Laboratories) and tissues were then counterstained with hematoxylin.

For TUNEL immunofluoresence staining, tissue sections were stained for apoptosis using the In Situ Cell Death Detection Kit, TMR red and following its protocol (Roche).

Chromatin Immunoprecipitation Assay—ChIP assays were performed on U87-EGFR cells +/− 4 hours of EGF treatment (20 ng/mL). Cells in two 15 cm plates were pooled for each

replicate. ChIP was performed essentially as described (37). Briefly, cells were crosslinked for 5 minutes in 1% formaldehyde in PBS. After extensive sonication (10 minutes total sonication time in 30 second pulses), pre-clearing with protein-G sepharose, and removal of a 50 uL (1/20 input) fraction for normalization, soluble chromatin from each replicate was split three ways for overnight immunoprecipitations with 2 ug of the following antibodies: Mouse IgG (Millipore cat #12-371, nonspecific control), anti-Pol II (Millipore clone CTD4H8, cat #05-623, positive control), or anti-SREBP1 (clone 2A4 derived from ATCC hybridoma cat #CRL-2121). DNA-Protein complexes were pulled down by incubation for 2 hours with protein-G sepharose, washed, and processed as previously described. gDNA was assayed by qPCR with primers amplifying the FAS transcription start site, and a fragment upstream of the Transcription Start Site (TSS). qPCR values were normalized against the input gDNA content for each replicate. qPCR primers are FAS TSS f: CTCTCTGGCTCCCTCTAGGC, FAS TSS r: GATGGCCGCGGTTTAAATA, FAS up f: GTGGGGCTGGGACTGAG, and FAS up r: CAGTGTGGCCCAAGCATT.

Xenograft Model—Isogenic human U87 malignant glioma cells (U87, U87-EGFRvIII) were implanted into immunodeficient SCID/Beige mice for subcutaneous (s.c.) xenograft studies. SCID/Beige mice were bred and kept under defined-flora pathogen-free conditions at the AALAC-approved Animal Facility of the Division of Experimental Radiation Oncology, UCLA. For s.c. implantation, exponentially growing tumor cells in culture were trypsinized, enumerated by Trypan Blue exclusion, and resuspended at 1×10^6 cells/ml in a solution of dPBS and Matrigel (BD Biosciences). Tumor growth was monitored with calipers by measuring the perpendicular diameters of each s.c. tumor. U87 and U87-EGFRvIII cell lines were implanted s.c. on opposite sides of the mouse abdomen (n=20) for treatment with atorvastatin (10 mg/kg daily; Toronto Research Chemicals, Canada), C75 (30 mg/kg weekly; Sigma, Saint Louis, MO) alone or in combination. Mice were euthanized if tumors reached 14 mm in maximum diameter, or animals showed signs of illness. All experiments were conducted after approval by the Chancellor's Animal Research Committee of UCLA.

Immunohistochemistry and image analysis-based scoring—Tissue sections were cut from blocks of formalin-fixed paraffin tumor tissue from glioblastoma patients treated with lapatinib or rapamycin. Tumor specimens were obtained according to a protocol approved by the Institutional Review Board of UCLA. The first set of paired pre- and post-treatment tumor tissues (n=9) for lapatinib trial, and 9 pairs of pre- and post-treatment tumor tissues for the rapamycin trial, were examined. Control group included 12 patient tumor tissues. Five-micron tissue sections were stained with polyclonal antibodies directed against p-EGFR Tyr^{1086}, p-Met Tyr^{1349}, p-PDGFR Tyr^{579}, p-AKT Ser^{473} and SREBP-1, ACC, FAS for sections of lapatinib trial and tissue microarray; and p-EGFR, p-AKT, SREBP-1 and p-S6 $Ser^{235/236}$ for sections of rapamycin trial. Digital scores for p-EGFR, p-AKT, and p-S6 were based on absolute staining intensity of tumor cells as quantified following false-color conversion. Sections were photographed using a Colorview II camera mounted on an Olympus BX41 microscope at 20× magnification. 5 images were captured per slide from representative regions of the tumor. Borders between individual cells were approximated using a separator function of the Soft Imaging Software (with the parameter of Smooth and Fine/Coarse, 2 and 10 respectively). Quantitative analysis was done using HSI color algorithm based on hue, saturation and intensity. Saturations of the separated cell in the images were quantified in the red-brown hue range to exclude the negative staining area with hematoxylin nuclear staining. To compare the staining intensity of all slides, mean saturation of total cells on each image was quantified and calculated. 1500 to 2000 cells per case (on average) were measured for each slide and statistical comparisons were performed using R software, using an approach previously described (14). For SREBP-1 staining scoring, separated cells were quantified with

red brown hue range (cells with positive nuclear staining) and total hue range (all cells) after cell border separation and proportion of positive cells was calculated based on these numbers.

Statistical Analysis—Results are shown as mean ± SEM. Fishers exact test was used to assess correlations between various molecular markers. Other comparisons in cell growth assays, tumor volumes, tumor metabolism and cell death were performed using two-tailed *t* test as well as by ANOVA as appropriate. We used Wilcoxon test to determine the *P*-value for staining of lapatinib trial pre-and post- treatment tissue samples. $P<0.05$ was considered as statistically significant. The computation of the Pearson correlations and the logistic regression analysis were all carried out with the R software. To depict the relationship between the variables, we used the R function cmd scale to arrive at a two-dimensional classical MDS plot. We also followed the convention of path analysis to represent a causal model by a directed graph and used partial correlation testing to fit a causal model.

Supplementary Material

Refer to Web version on PubMed Central for supplementary material.

References and Note

1. Stupp R, Mason WP, van den Bent MJ, Weller M, Fisher B, Taphoorn MJ, Belanger K, Brandes AA, Marosi C, Bogdahn U, Curschmann J, Janzer RC, Ludwin SK, Gorlia T, Allgeier A, Lacombe D, Cairncross JG, Eisenhauer E, Mirimanoff RO. Radiotherapy plus concomitant and adjuvant temozolomide for glioblastoma. N Engl J Med 2005;352:987–996. [PubMed: 15758009]
2. Furnari FB, Fenton T, Bachoo RM, Mukasa A, Stommel JM, Stegh A, Hahn WC, Ligon KL, Louis DN, Brennan C, Chin L, DePinho RA, Cavenee WK. Malignant astrocytic glioma: genetics, biology, and paths to treatment. Genes Dev 2007;21:2683–2710. [PubMed: 17974913]
3. Comprehensive genomic characterization defines human glioblastoma genes and core pathways. Nature 2008;455:1061–1068. [PubMed: 18772890]
4. Bublil EM, Yarden Y. The EGF receptor family: spearheading a merger of signaling and therapeutics. Curr Opin Cell Biol 2007;19:124–134. [PubMed: 17314037]
5. Schlessinger J. Cell signaling by receptor tyrosine kinases. Cell 2000;103:211–225. [PubMed: 11057895]
6. Rich JN, Reardon DA, Peery T, Dowell JM, Quinn JA, Penne KL, Wikstrand CJ, Van Duyn LB, Dancey JE, McLendon RE, Kao JC, Stenzel TT, Ahmed Rasheed BK, Tourt-Uhlig SE, Herndon E 2nd, Vredenburgh JJ, Sampson JH, Friedman AH, Bigner DD, Friedman HS. Phase II trial of gefitinib in recurrent glioblastoma. J Clin Oncol 2004;22:133–142. [PubMed: 14638850]
7. Mellinghoff IK, Wang MY, Vivanco I, Haas-Kogan DA, Zhu S, Dia EQ, Lu KV, Yoshimoto K, Huang JH, Chute DJ, Riggs BL, Horvath S, Liau LM, Cavenee WK, Rao PN, Beroukhim R, Peck TC, Lee JC, Sellers WR, Stokoe D, Prados M, Cloughesy TF, Sawyers CL, Mischel PS. Molecular determinants of the response of glioblastomas to EGFR kinase inhibitors. N Engl J Med 2005;353:2012–2024. [PubMed: 16282176]
8. Haas-Kogan DA, Prados MD, Tihan T, Eberhard DA, Jelluma N, Arvold ND, Baumber R, Lamborn KR, Kapadia A, Malec M, Berger MS, Stokoe D. Epidermal growth factor receptor, protein kinase B/Akt, and glioma response to erlotinib. J Natl Cancer Inst 2005;97:880–887. [PubMed: 15956649]
9. Stommel JM, Kimmelman AC, Ying H, Nabioullin R, Ponugoti AH, Wiedemeyer R, Stegh AH, Bradner JE, Ligon KL, Brennan C, Chin L, DePinho RA. Coactivation of receptor tyrosine kinases affects the response of tumor cells to targeted therapies. Science 2007;318:287–290. [PubMed: 17872411]
10. Weihua Z, Tsan R, Huang WC, Wu Q, Chiu CH, Fidler IJ, Hung MC. Survival of cancer cells is maintained by EGFR independent of its kinase activity. Cancer Cell 2008;13:385–393. [PubMed: 18455122]

11. Kong A, Calleja V, Leboucher P, Harris A, Parker PJ, Larijani B. HER2 oncogenic function escapes EGFR tyrosine kinase inhibitors via activation of alternative HER receptors in breast cancer cells. PLoS ONE 2008;3:e2881. [PubMed: 18682844]
12. Guix M, Faber AC, Wang SE, Olivares MG, Song Y, Qu S, Rinehart C, Seidel B, Yee D, Arteaga CL, Engelman JA. Acquired resistance to EGFR tyrosine kinase inhibitors in cancer cells is mediated by loss of IGF-binding proteins. J Clin Invest 2008;118:2609–2619. [PubMed: 18568074]
13. Engelman JA, Settleman J. Acquired resistance to tyrosine kinase inhibitors during cancer therapy. Curr Opin Genet Dev 2008;18:73–79. [PubMed: 18325754]
14. Cloughesy TF, Yoshimoto K, Nghiemphu P, Brown K, Dang J, Zhu S, Hsueh T, Chen Y, Wang W, Youngkin D, Liau L, Martin N, Becker D, Bergsneider M, Lai A, Green R, Oglesby T, Koleto M, Trent J, Horvath S, Mischel PS, Mellinghoff IK, Sawyers CL. Antitumor activity of rapamycin in a Phase I trial for patients with recurrent PTEN-deficient glioblastoma. PLoS Med 2008;5:e8. [PubMed: 18215105]
15. Choe G, Horvath S, Cloughesy TF, Crosby K, Seligson D, Palotie A, Inge L, Smith BL, Sawyers CL, Mischel PS. Analysis of the phosphatidylinositol 3'-kinase signaling pathway in glioblastoma patients in vivo. Cancer Res 2003;63:2742–2746. [PubMed: 12782577]
16. DeBerardinis RJ, Lum JJ, Hatzivassiliou G, Thompson CB. The biology of cancer: metabolic reprogramming fuels cell growth and proliferation. Cell Metab 2008;7:11–20. [PubMed: 18177721]
17. Goldstein JL, Brown MS. From fatty streak to fatty liver: 33 years of joint publications in the JCI. J Clin Invest 2008;118:1220–1222. [PubMed: 18382725]
18. Horton JD, Goldstein JL, Brown MS. SREBPs: activators of the complete program of cholesterol and fatty acid synthesis in the liver. J Clin Invest 2002;109:1125–1131. [PubMed: 11994399]
19. Porstmann T, Santos CR, Griffiths B, Cully M, Wu M, Leevers S, Griffiths JR, Chung YL, Schulze A. SREBP activity is regulated by mTORC1 and contributes to Akt-dependent cell growth. Cell Metab 2008;8:224–236. [PubMed: 18762023]
20. Wang SL, Du EZ, Martin TD, Davis RA. Coordinate regulation of lipogenesis, the assembly and secretion of apolipoprotein B-containing lipoproteins by sterol response element binding protein 1. J Biol Chem 1997;272:19351–19358. [PubMed: 9235933]
21. Yang J, Sato R, Goldstein JL, Brown MS. Sterol-resistant transcription in CHO cells caused by gene rearrangement that truncates SREBP-2. Genes Dev 1994;8:1910–1919. [PubMed: 7958866]
22. Espenshade PJ, Hughes AL. Regulation of sterol synthesis in eukaryotes. Annu Rev Genet 2007;41:401–427. [PubMed: 17666007]
23. Bengoechea-Alonso MT, Ericsson J. SREBP in signal transduction: cholesterol metabolism and beyond. Curr Opin Cell Biol 2007;19:215–222. [PubMed: 17303406]
24. Agulnik MM, da Cunha Santos G, Hedley D, Nicklee T, Dos Reis PP, Ho J, Pond GR, Chen H, Chen S, Shyr Y, Winquist E, Soulieres D, Chen EX, Squire JA, Marrano P, Kamel-Reid S, Dancey J, Siu LL, Tsao MS. Predictive and pharmacodynamic biomarker studies in tumor and skin tissue samples of patients with recurrent or metastatic squamous cell carcinoma of the head and neck treated with erlotinib. J Clin Oncol 2007;25:2184–2190. [PubMed: 17538163]
25. Nagane M, Coufal F, Lin H, Bogler O, Cavenee WK, Huang HJ. A common mutant epidermal growth factor receptor confers enhanced tumorigenicity on human glioblastoma cells by increasing proliferation and reducing apoptosis. Cancer Res 1996;56:5079–5086. [PubMed: 8895767]
26. Kroemer G, Pouyssegur J. Tumor cell metabolism: cancer's Achilles' heel. Cancer Cell 2008;13:472–482. [PubMed: 18538731]
27. Engelman JA, Cantley LC. A sweet new role for EGFR in cancer. Cancer Cell 2008;13:375–376. [PubMed: 18455118]
28. Shaw RJ. Glucose metabolism and cancer. Curr Opin Cell Biol 2006;18:598–608. [PubMed: 17046224]
29. Kalaany NY, Sabatini DM. Tumours with PI3K activation are resistant to dietary restriction. Nature 2009;458:725–731. [PubMed: 19279572]
30. Migita T, Ruiz S, Fornari A, Fiorentino M, Priolo C, Zadra G, Inazuka F, Grisanzio C, Palescandolo E, Shin E, Fiore C, Xie W, Kung AL, Febbo PG, Subramanian A, Mucci L, Ma J, Signoretti S, Stampfer M, Hahn WC, Finn S, Loda M. Fatty acid synthase: a metabolic enzyme and candidate oncogene in prostate cancer. J Natl Cancer Inst 2009;101:519–532. [PubMed: 19318631]

31. Guo D, Hildebrandt IJ, Prins RM, Soto H, Mazzotta MM, Dang J, Czernin J, Shyy JY, Watson AD, Phelps M, Radu CG, Cloughesy TF, Mischel PS. The AMPK agonist AICAR inhibits the growth of EGFRvIII-expressing glioblastomas by inhibiting lipogenesis. Proc Natl Acad Sci U S A 2009;106:12932–12937. [PubMed: 19625624]

32. Kaelin WG Jr. The concept of synthetic lethality in the context of anticancer therapy. Nat Rev Cancer 2005;5:689–698. [PubMed: 16110319]

33. Hsieh S, Tobien T, Koch K, Dunn J. Increasing throughput of parallel on-line extraction liquid chromatography/electrospray ionization tandem mass spectrometry system for GLP quantitative bioanalysis in drug development. Rapid Commun Mass Spectrom 2004;18:285–292. [PubMed: 14755613]

34. Guo D, Chien S, Shyy JY. Regulation of endothelial cell cycle by laminar versus oscillatory flow: distinct modes of interactions of AMP-activated protein kinase and Akt pathways. Circ Res 2007;100:564–571. [PubMed: 17272808]

35. Watson AD. Thematic review series: systems biology approaches to metabolic and cardiovascular disorders. Lipidomics: a global approach to lipid analysis in biological systems. J Lipid Res 2006;47:2101–2111. [PubMed: 16902246]

36. Lu KV, Zhu S, Cvrljevic A, Huang TT, Sarkaria S, Ahkavan D, Dang J, Dinca EB, Plaisier SB, Oderberg I, Lee Y, Chen Z, Caldwell JS, Xie Y, Loo JA, Seligson D, Chakravari A, Lee FY, Weinmann R, Cloughesy TF, Nelson SF, Bergers G, Graeber T, Furnari FB, James CD, Cavenee WK, Johns TG, Mischel PS. Fyn and SRC are effectors of oncogenic epidermal growth factor receptor signaling in glioblastoma patients. Cancer Res 2009;69:6889–6898. [PubMed: 19690143]

37. Villena JA, Hock MB, Chang WY, Barcas JE, Giguere V, Kralli A. Orphan nuclear receptor estrogen-related receptor alpha is essential for adaptive thermogenesis. Proc Natl Acad Sci U S A 2007;104:1418–1423. [PubMed: 17229846]

38. We thank George Thomas, Caius Radu, Johannes Czernin, Owen Witte and Peter Edwards for helpful discussions. This work was supported by the National Institute for Neurological Disorders and Stroke (NS050151) and the National Cancer Institute (CA119347 and CA108633), and the Brain Tumor Funders' Collaborative. This work was also supported by the Harry Allgauer Foundation through The Doris R. Ullman Fund for Brain Tumor Research Technologies, the Henry E. Singleton Brain Tumor Program, and generous donations from the Ziering Family Foundation in memory of Sigi Ziering and Timothy and Mary Hahneman. We acknowledge institutional investigators from NABTC 04-01 A Biomarker and Phase II study of GW 572016 in Recurrent Malignant Glioma: Howard Fine, Susan Chang, Frank Lieberman, David Reardon, Lauren Abrey, Andrew Lassman, Kenneth Aldape, WK Alfred Yung, Janet Dancey, and Kathleen Lamborn. Grant support: for the Lapatinib Trial: University of Texas Health Science Center (San Antonio, TX) grants UO1CA62426 and P30CA54174, University of California at San Francisco grants U01CA62422 and GCRC# M01-RR00079, Dana-Farber Cancer Center grant U01CA62407, University of California at Los Angeles grants U01CA62339 and GCRC# M01-RR0865, University of Wisconsin Hospital grants U01CA62421 and GCRC# M01-RR03186, and Memorial Sloan-Kettering Cancer Center grant U01CA62399, University of Texas M. D. Anderson Cancer Center grants CA62412 and CA16672, University of Pittsburgh NABTC grant CA 62404 and GCRC grant M01-RR00056.

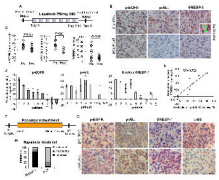

Fig. 1.

EGFR and Akt signaling and nuclear SREBP-1 accumulation response data in the first set of 9 GBM patients receiving lapatinib in a Phase II clinical trial. (**A**) Tumor tissue was analyzed from 9 GBM patients before and after treatment with the EGFR inhibitor lapatinib. (**B**) Immunohistochemical staining (reddish brown) of phospho-EGFR Tyr^{1086}, phospho-Akt Ser^{473} and SREBP-1 before and after treatment with lapatinib from a representative patient (#1). Nuclei were counterstained with hematoxylin (blue). Inset shows nuclear SREBP-1 staining indicated by green arrow. Scale bar = 20 um. (**C**) Quantification of immunohistochemical staining from >1000 cells from at least five representative areas of each tumor before and after lapatinib treatment, *P*-values were determined by Wilcoxon text (7). Each diamond represents an individual patient. (**D**) Reduction of p-EGFR, p-Akt and nuclear SREBP-1 staining for each GBM patient before (S1) and after (S2) treatment with lapatinib. (**E**) Correlation between inhibition of p-EGFR and inhibition of nuclear SREBP-1 staining. (**F**) Analysis of tumor tissue from 9 GBM patients before and after treatment with rapamycin. (**G**) Immunohistochemical staining (reddish brown) of p-EGFR Tyr^{1086}, p-Akt Ser^{473}, SREBP-1 and p-S6 $Ser^{235/236}$ before and after treatment with rapamycin. (**H**) Percentage of patients with decreased nuclear SREBP-1 staining and percentage of patients with decreased p-S6 staining. Scale bar = 20 um.

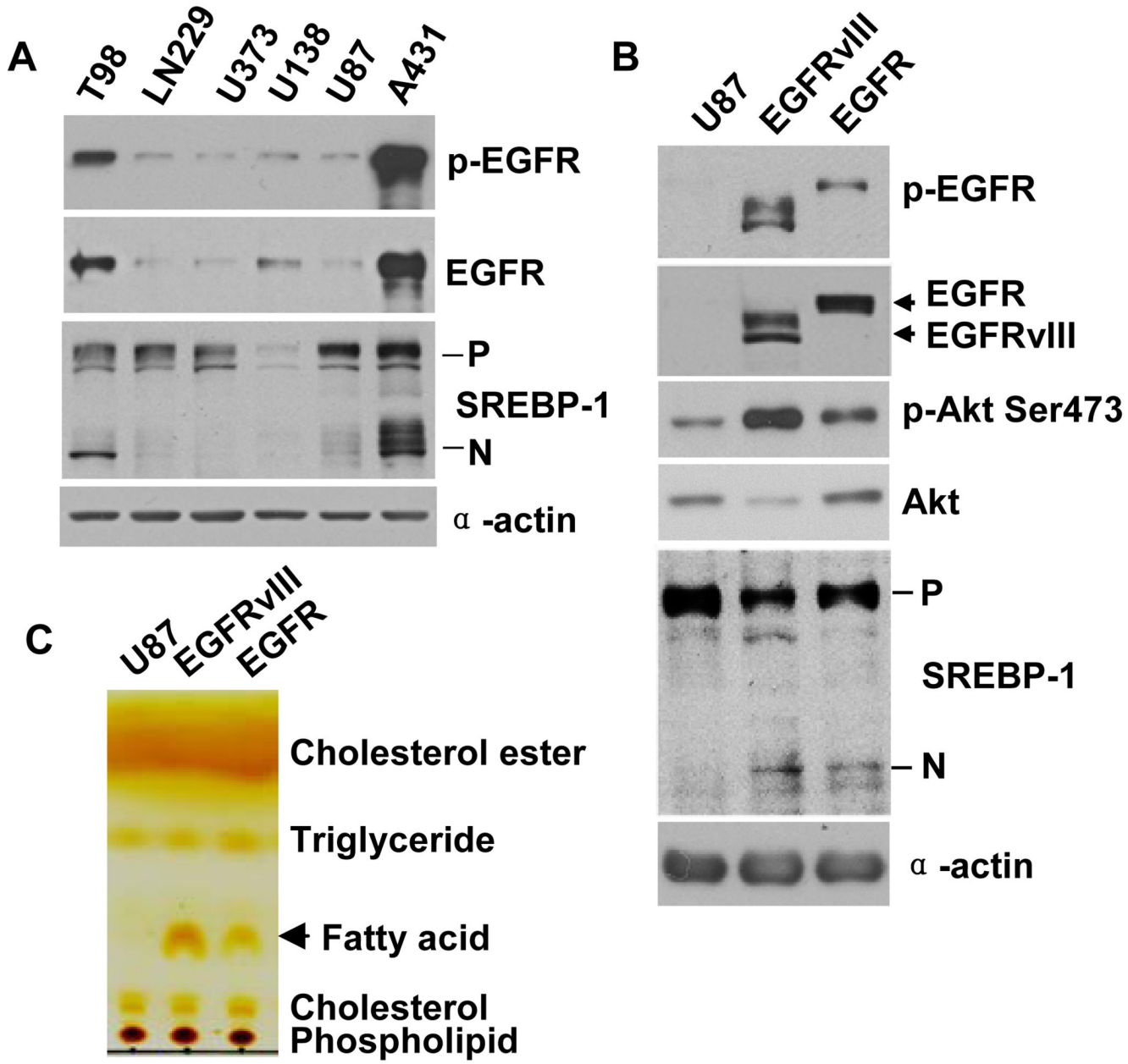

Fig. 2.

Increased SREBP-1 cleavage and fatty acid accumulation in GBM cell lines correlates with abundant EGFR-PI3K-Akt signaling. (**A**) Western blot analysis of lysates from cell lines cultured in medium containing 1% FBS. For SREBP-1 immunoblot, P=Precursor; N=cleaved NH2 terminal form. α-actin used as loading control. (**B**) Biochemical analysis of effect of transfection of EGFRvIII or wild-type EGFR on SREBP-1 cleavage compared with parental U87 GBM cells that endogenously contain little EGFR and no EGFRvIII. Cell lines were cultured in serum-free media for 48 hrs. (**C**) Total lipid extracts from U87 GBM cells, with or without EGFRvIII or EGFR over-expression, cultured in serum-free media for 48 hours were subjected to thin layer chromatography and visualized by iodine.

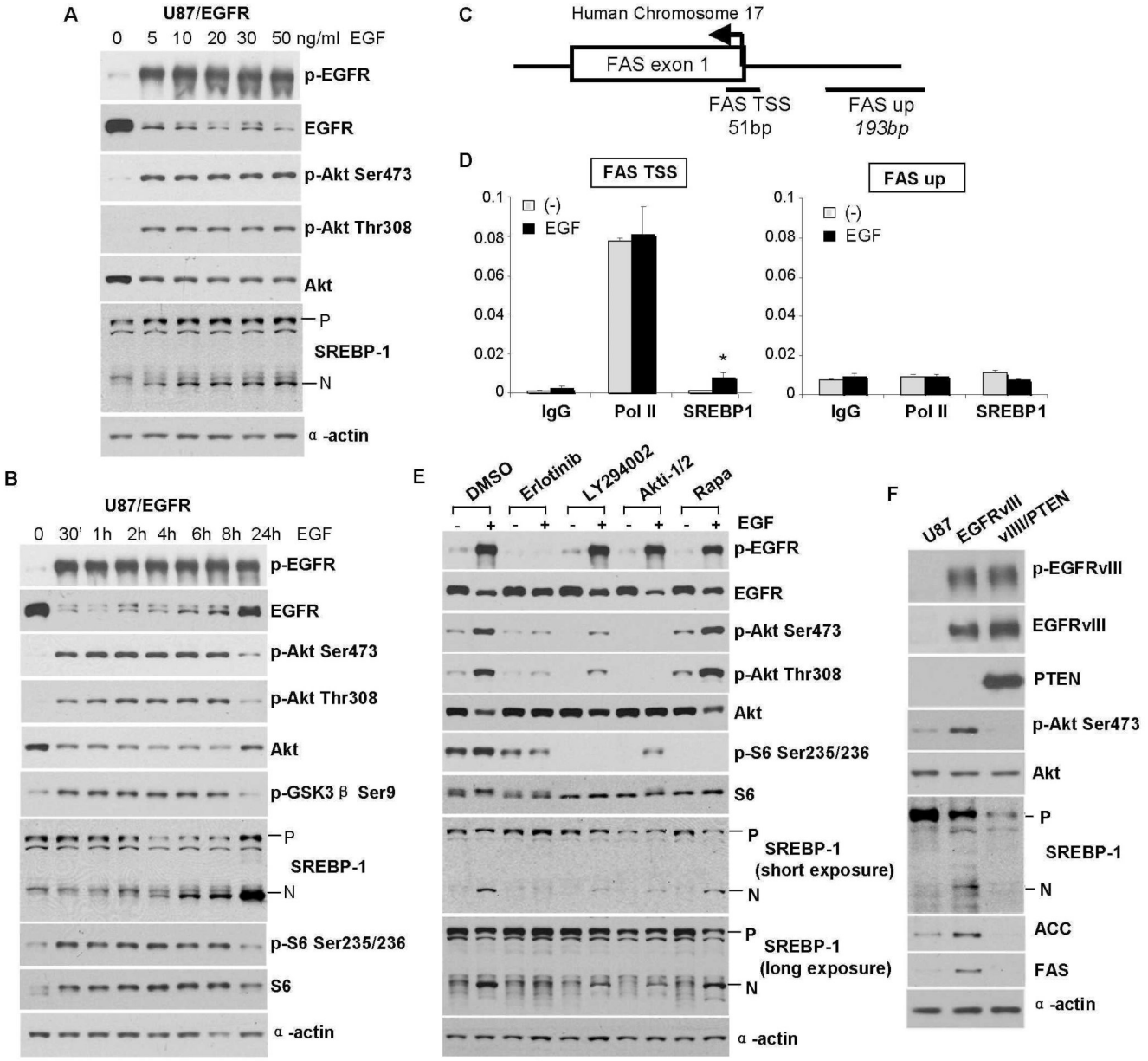

Fig. 3.

Pharmacologic and genetic manipulation of GBM cells demonstrates that EGFR-PI3K-Akt signaling promotes SREBP-1 cleavage and binding to the FAS promoter (**A**) Effect of EGF dose, and time course of EGF effect on SREBP-1 cleavage (**B**). U87-EGFR GBM cells were cultured in serum-free medium for 24 hrs and treated for 6 hrs with indicated concentration of EGF or with EGF (20 ng/ml) in time course experiments. Immunoblot analysis was performed with indicated antibodies. Antibodies against total proteins recognize both phosphorylated and nonphosphorylated proteins. (**C**) A schematic depicting the human FAS locus and approximate locations of the qPCR amplicons. TSS represents transcription start site. Up represents a site 200 base pairs upstream. (**D**) SREBP-1 abundance at the FAS transcription start site increases in response to EGF treatment. Chromatin immunoprecipitation was performed on U87-EGFR cells with EGF (20 ng/mL) for 4 hrs. Data are normalized against a fraction of the input gDNA, and each bar represents the mean +/− SEM of three independent biologic replicates. * P= 0.02

relative to non-EGF treated samples. (**E**) Effect of the EGFR inhibitor erlotinib (10 uM), the PI3K inhibitor LY294002 (20 uM), Akt inhibitor Akti-1/2 (5 uM) or rapamycin (1 nM) for 16 hours on SREBP-1 cleavage in U87-EGFR cells. (**F**) Effect of PTEN reconstitution on EGFRvIII-mediated SREBP-1 cleavage, and ACC and FAS abundance.

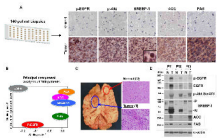

Fig. 4.

p-EGFR is associated with p-Akt, nuclear SREBP-1 and increased abundance of ACC and FAS in a cohort of 140 GBM patients. (**A**) Analysis of p-EGFR, p-Akt, nuclear SREBP-1, and FAS and ACC abundance (reddish brown) in two tissue microarrays comprising 252 tumor cores and 91 matched normal cores from 140 primary (*de novo*) GBM patients. Inset demonstrates nuclear SREBP-1 staining. Images are 20×, tissue is counterstained with hematoxylin. Scale bar = 20 um. (**B**) Multidimensional scaling plot based on correlations between EGFR, p-EGFR Tyr^{1086}, p-Akt Ser^{473}, nuclear SREBP-1, ACC and FAS. (**C**) Representative gross and microscopic pictures of tumor tissue (T) and contralateral normal brain tissue (N) from the brain of a GBM patient obtained at autopsy. Scale bar = 20 um. (**D**) Immunoblot analysis of p-EGFR, p-Akt, SREBP-1 cleavage, and ACC and FAS abundance in tumor (T) and contralateral normal brain tissue (N) from for three GBM patients obtained at autopsy.

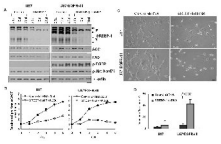

Fig. 5.

ShRNA knock down of SREBP-1 promotes extensive tumor cell death of EGFRvIII-bearing GBM cells. (**A**) Immunoblot analysis demonstrating shRNA knockdown of SREBP-1 in U87 and U87-EGFRvIII GBM cells. SREBP-1 abundance was substantially reduced 48 hours after shRNA lentiviral infection. Cell lysates were analyzed by Western blot using the indicated antibodies. (**B**) Cells were infected with SREBP-1 shRNA lentivirus or scrambled control shRNA lentivirus for 24 hrs, subcultured into 96 well plates, and changed to 1% FBS medium after 24 hrs. Relative cell proliferation was assayed daily until day 5 using the WST assay (Chemicon). (**C, D**) Cells were infected with SREBP-1 shRNA lentivirus or scrambled control for 24 hrs, split into 12 well plates and change to 1% FBS medium for 4 days after 24 hrs. Cell morphology was imaged using a phase contrast invert-microscope and digital camera and cell death was measured by trypan blue exclusion. Scale bar = 20 um.

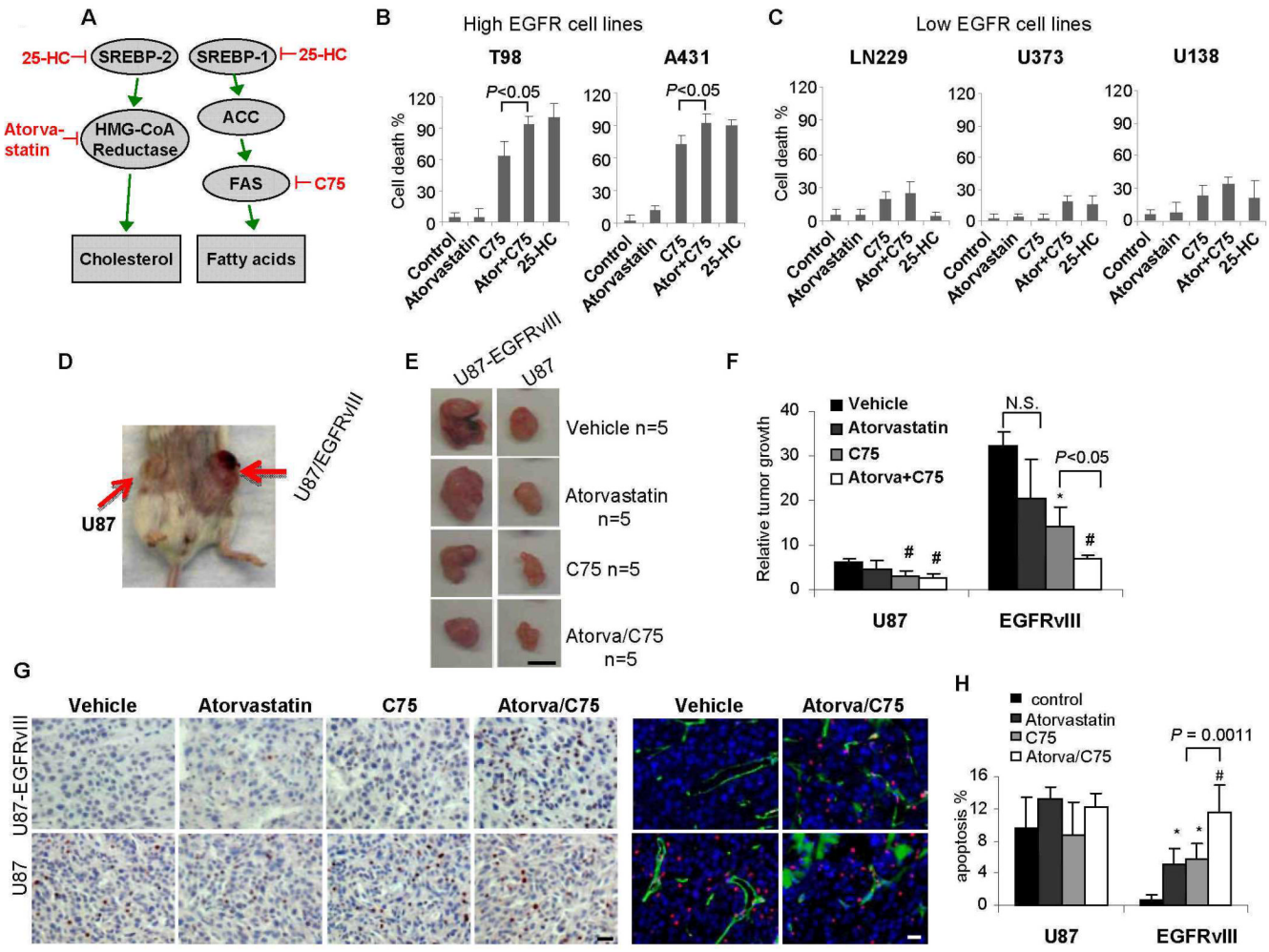

Fig. 6.

A constitutively active form of the EGFR allele is sufficient to sensitize GBMs in vitro and in vivo to apoptotic cell death in response to fatty acid synthase inhibition. (**A**) Schematic view of inhibitors. (**B**) Effect of the FAS inhibitor C75 (10 μg/ml) and the HMG-CoA reductase inhibitor atorvastatin (1 μM), alone or in combination in EGFR-high GBM cell lines relative to (**C**) EGFR-low cell lines. Cell death was measured by trypan blue exclusion. (**D**) In vivo model in which U87 cells, or U87 cells transfected with EGFRvIII were subcutaneously implanted in the flank of immunocompromised mice. EGFRvIII-bearing tumors are significantly larger. (**E**) Effect of C75 (30 mg/kg weekly) or atorvastatin (10 mg/kg daily) alone or in combination. Scale bar = 1mm. (**F**) Quantification of the effect on tumor size. # $P<0.05$ compared with vehicle treated tumor volume; * $P<0.05$ compared with vehicle treated tumor volume; N.S. means no significant. (**G**) Representative images demonstrating TUNEL staining to assess apoptotic effect. Scale bar = 20 um. (**H**) Quantification of TUNEL staining. * $P<0.01$ compared with vehicle treated tumor; # $P<0.0001$ compared with vehicle treated tumor.

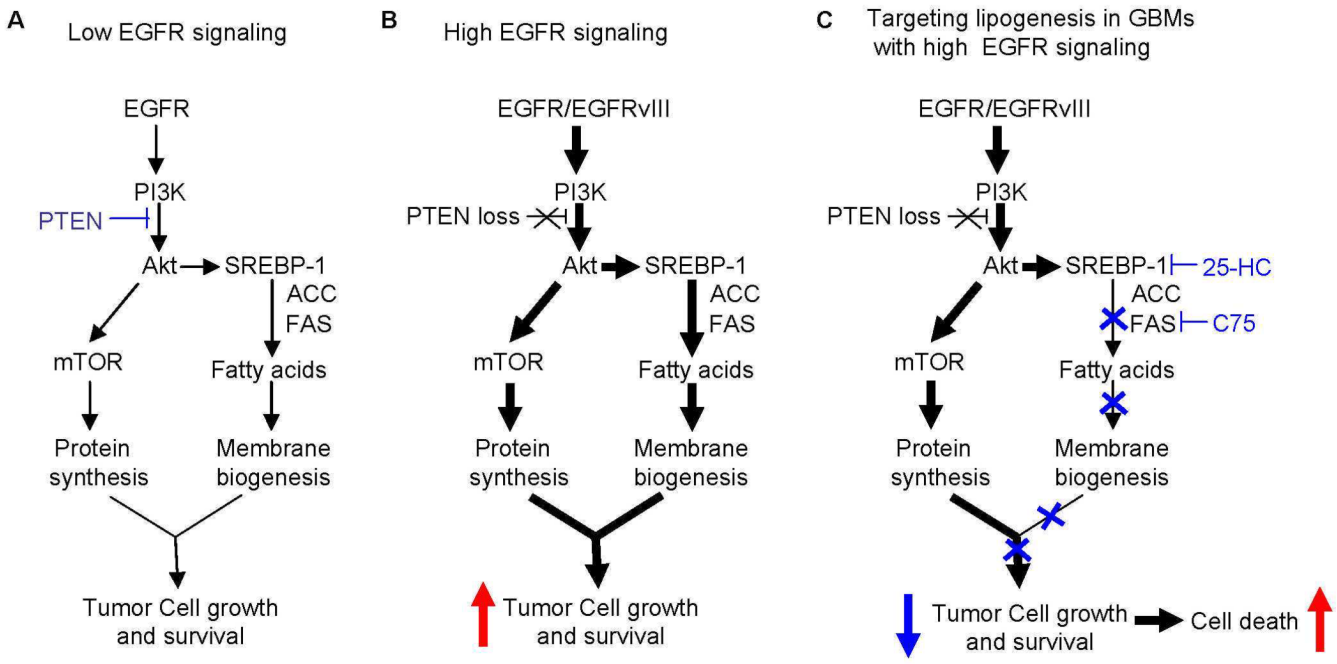

Fig. 7.

Model demonstrating the specific apoptotic effect of SREBP-1 and FAS inhibition on GBM cells bearing EGFRvIII. (**A**) In cells with little EGFR and intact PTEN, the demand for lipogenesis is modest and is balanced by low levels of SREBP-1 pathway activation. (**B**) In GBM cells with abundant EGFR and PTEN loss, the SREBP-1-ACC-FAS pathway is upregulated to meet the demand for increased fatty acid synthesis for membrane biogenesis of rapidly dividing cancer cells. (**C**) The SREBP-1 pathway becomes essential for survival in GBM cells bearing EGFRvIII. Targeting SREBP-1 or FAS is therefore lethal to EGFRvIII-bearing GBM cells.